

Analytical modeling of large-scale bioreactors using diffusion equations: Perspectives on bioprocess design

Pauli Sakari Losoi

Short title: Analytical modeling of large-scale bioreactors using diffusion equations

Note: An oral presentation of this paper's topic was meant to be given at the 8th BioProScale Symposium 9th April 2024, but the author unfortunately was hindered from attending and delivering the talk.

Corresponding author: Pauli Sakari Losoi, Faculty of Engineering and Natural Sciences, Tampere University, pauli.losoi@tuni.fi, +358504751062, Korkeakoulunkatu 8, 33720 Tampere, Finland

Abstract

BACKGROUND: Modeling is a widely employed tool in the study of bioreactor scale-up where mixing, reaction, mass transfer, and biological phenomena interact. Heterogeneous large-scale reactors have usually been modeled with numerical models which naturally employ an analysis workflow of determining an end result from operating conditions. Design perspective that uses the desired end result to infer the required operating conditions is usually not accounted for.

RESULTS: To fill this gap, one-dimensional axial diffusion equations have been proposed as a generalized model of high aspect ratio bioreactors. Using a previously published large-scale *Escherichia coli* fed-batch as a reference and a previously published kinetic model, the design perspective was demonstrated by using the analytically solved diffusion equation model to determine maximal mixing times and feed rates that avoid acetate overflow. Similarly, the minimum required oxygen transfer rate coefficients and oxygen gas partial pressures for the same scenario were determined.

CONCLUSION: Analytical solutions to axial diffusion equations could be used for preliminary quick screening of process parameters required to fulfill a design objective. In future, the model could be used to initialize more involved numerical simulations or in the design of scale-down setups mimicking the environment found in large-scale reactors.

Keywords

bioreactor, bioprocess, modeling, scale-up, diffusion equation

1 Introduction

Non-homogeneous conditions are characteristic of large-scale bioreactors, where the fed substrate, dissolved gases, pH, and temperature may be heterogeneously distributed¹. In effect, the host microorganism may activate various stress responses to temperature changes² and extremes of pH³, osmotic pressure⁴, oxygen⁵, and carbon dioxide⁶. Heterogeneity of the microorganism-affecting quantities is often considered detrimental⁷, as it is associated with lower yields and productivities⁸. However, heterogeneity is not only a negative feature: depending on the context, host viability⁷, product quality^{9,10}, and yield and productivity^{11,12} may be improved by the heterogeneous conditions. Ideally, experiments would be conducted to characterize the production host and the whole process at the large scale, but for economical and practical reasons such experiments are rare and inaccessible for most, thus necessitating modeling and simulations.

Apart from correlations and homogeneous ideal reactor models, modeling of bioreactors has thus far been mostly numerical in nature, being based on compartment models^{13–17} and computational fluid dynamics simulations^{18–21}. The previous modeling studies have analyzed various bioreactor scenarios and produced profiles of substrate and dissolved gases based on chosen operating conditions. The focus has been on analysis of existing scenarios and how the host microorganism's metabolism is affected. However, the process design perspective that starts with the desired end result²², has usually been left unexplored in modeling. Instead of focusing on, for example, how much of overflow metabolism²³ *Escherichia coli* is expected to exhibit under the analyzed scenario, and how large a biomass yield loss is expected as a result, one could ask what should the mixing time or the glucose feed rate be to avoid the acetate overflow and biomass yield loss of *E. coli* altogether. Similarly, one could determine how large an oxygen transfer rate is required to avoid dissolved oxygen limitations at the feed point's vicinity, instead of analyzing the extent of the oxygen limitation itself. These design questions are in opposition to the typical numerical workflow, where the operating conditions are used to determine the end result. In contrast, the design perspective infers the operating conditions using a predefined desired end result as the starting point.

For screening of such preliminary process design choices, less involved, directly computable models would be preferable. A recent two-part study^{24,25} demonstrated that typical large-scale stirred bioreactors with high aspect ratios can be modeled with analytically solved 1D diffusion equations, which are essentially continuous 1D formulations of earlier 1D and 2D compartment models^{26,27}. Similarly to the more involved simulation approaches, the 1D diffusion equation models have been used to analyze profiles of substrate, dissolved oxygen and carbon dioxide, temperature, and pH in large-scale reactors. The aim of this work is to demonstrate how the design perspective can be satisfied using 1D diffusion equation based models of large-scale bioreactors. A reference fed-batch culture from literature⁸ is used as an example case, and the maximal mixing times and substrate feed rates that avoid acetate accumulation according to a kinetic model²⁸ are determined. In addition, the minimum required oxygen transfer rate coefficients and oxygen gas partial pressures are calculated for the same example scenario. Also, clear operating instructions—simple enough to be carried out even in spreadsheet software—are provided, which is a major simplification in comparison with earlier simulations.

2 Materials and methods

2.1 Diffusion equation modeling

The diffusion equation based model is in essence a continuous form of 1D compartment models^{13,26}, where the axial mixing is represented by a diffusion constant, the dispersion coefficient d ($\text{m}^2 \text{s}^{-1}$). The other way around, 1D compartment models are coarse-grained discretizations of 1D diffusion equations. The model

development has been presented earlier^{24,25}, and only the main results necessary for the model application are reviewed here.

The model couples the mixing times t_u (s) at a threshold level of homogeneity $|1 - u|$ with the geometry and dispersion coefficient²⁴:

$$t_u = \frac{H^2}{\pi^2 d} \ln \frac{2 \cos(\pi x_0) \cos(\pi x)}{1 - u}. \quad (1)$$

H is the working height (m), u the dimensionless tracer concentration, x the axial coordinate divided by height ($x = 1$ is at the top of the working volume), and x_0 the feed point's dimensionless axial coordinate. In particular, the dispersion coefficient d is related to the most commonly used 95 % mixing time t_{95} (normalized tracer concentration within 5 % of equilibrium) by

$$d = \frac{\ln 40}{\pi^2} \frac{H^2}{t_{95}}, \quad (2)$$

when the measurement and feed points are as far apart as possible (at the very top or bottom). If either the feed point or the mixing time measurement point is close to the middle of the reactor, another form of the shown equations needs to be used according to the previous study²⁴. Eqn 2 can be utilized if a mixing time is known or an applicable mixing time correlation exists. If the mixing time is not known and no specific correlation exists, a predictive method for determining the dispersion coefficient validated with a large set of data²⁴ can be used.

The axially variable substrate concentration S (g L^{-1}) is related to the substrate's mean concentration (g L^{-1}) by²⁵

$$S = \langle S \rangle \frac{M}{\sinh M} \cosh(M \min(x, x_0)) \cosh(M(1 - \max(x, x_0))). \quad (3)$$

The dimensionless substrate modulus, M , is the square root of the ratio of the time-scales of reaction ($r_S / \langle S \rangle$) and mixing (H^2 / d):

$$M = H \sqrt{\frac{r_S / \langle S \rangle}{d}}, \quad (4)$$

where r_S is the overall volumetric substrate consumption rate ($\text{g L}^{-1} \text{h}^{-1}$). In a fed-batch, the substrate consumption rate can usually be approximated well enough by the substrate feed rate Q_S ($\text{g L}^{-1} \text{h}^{-1}$). In terms of the longest possible 95 % mixing time, the modulus is

$$M = \frac{\pi}{\sqrt{\ln 40}} \sqrt{t_{95} \frac{Q_S}{\langle S \rangle}} \quad (5)$$

with the $r_S \approx Q_S$ approximation.

The substrate's mean concentration $\langle S \rangle$ was estimated directly from Monod-kinetics²⁹ $r_S = q_S X \langle S \rangle / (\langle S \rangle + K_S) \approx Q_S$, yielding

$$\langle S \rangle = \frac{Q_S}{q_S X - Q_S} K_S, \quad (6)$$

where q_S is the maximum specific substrate uptake rate ($\text{g g}^{-1} \text{h}^{-1}$), X the biomass concentration (g L^{-1}), and K_S the Monod constant (g L^{-1}).

The local dissolved oxygen concentration was approximated to follow a steady-state balance equation without liquid-phase mixing:

$$k_L a (h_O O_G - O_L) = q_O X, \quad (7)$$

where $k_L a$ is the oxygen transfer rate coefficient (h^{-1}), $h_O = 0.0275 \text{ mol mol}^{-1}$ the Henry's constant for oxygen³⁰, O_G the concentration of oxygen in the gas phase (g L^{-1}), O_L the dissolved oxygen concentration (g L^{-1}), and q_O the specific oxygen consumption rate ($\text{g g}^{-1} \text{h}^{-1}$). The specific oxygen consumption rate q_O was made to depend on the local substrate concentration S (Eqn 3) according to a kinetic model.

2.2 Metabolic model and case example

An *E. coli* kinetic model²⁸ was applied here to relate the concentrations of substrate (glucose), acetate, and oxygen to the biomass-specific reaction rates. The maximum specific substrate uptake rate depended only on acetate concentration A (g L^{-1}):

$$q_S = \frac{0.6356 \text{ g g}^{-1} \text{h}^{-1}}{1 + A / (1.2399 \text{ g L}^{-1})}. \quad (8)$$

The actual substrate uptake rate was then obtained by multiplying q_S by the Monod-term $S / (S + (0.0370 \text{ g L}^{-1}))$. The net production or consumption of acetate depended on the substrate, acetate, and oxygen concentrations as explained in the original publication²⁸. The specific oxygen consumption rate was related to the substrate and acetate consumption rates as explained earlier²⁸.

A 22 m^3 *E. coli* fed-batch⁸ was used as a reference case. The reactor's total volume was 30 m^3 , and the working height was here assumed to be 7 m. A $t_{95} = 165 \text{ s}$ mixing time, $k_L a = 180 \text{ h}^{-1}$ oxygen transfer rate coefficient, and $\epsilon = 1.3 \text{ W kg}^{-1}$ specific stirrer power input was reported¹⁷ for the fermentation. The head-space pressure was reported⁸ to range between 1.25 bar and 1.5 bar. An absolute pressure of 2.5 bar was then used here for the head-space. Assuming a 1000 kg m^{-3} broth density, the absolute pressure at the bottom of the reactor was estimated to be 3.2 bar. The input air was assumed to contain 21 mol-% oxygen.

After the initial batch-phase, the reference fed-batch started with an exponential feed and continued with a constant feed. Both feeding schemes were considered here: (1) a constant $Q_S = 4 \text{ g L}^{-1} \text{h}^{-1}$, which resembles the one used in the referenced large-scale fed-batch culture⁸, (2) and an exponential feed

$$Q_S = (0.245 \text{ g g}^{-1} \text{h}^{-1}) X, \quad (9)$$

which corresponds to an exponential growth rate of 0.11 h^{-1} with 50% biomass yield on substrate and $0.025 \text{ g g}^{-1} \text{h}^{-1}$ maintenance rate³¹. The 0.11 h^{-1} specific growth rate was chosen to ensure aerobic growth according to the kinetic model²⁸. The exponential feed rate ranged from $0.98 \text{ g L}^{-1} \text{h}^{-1}$ to $9.8 \text{ g L}^{-1} \text{h}^{-1}$ as the biomass concentration ranged from 4 g L^{-1} to 40 g L^{-1} . In the referenced large-scale cultivation⁸, a 37 g L^{-1} biomass concentration was measured at the end of the process. Here, biomass concentrations from 4 g L^{-1} to 40 g L^{-1} were considered.

2.3 Software

All computations were performed with Python 3.11.7 using the packages NumPy 1.26.4³² and pandas 2.1.4^{33,34}. However, selected computations were implemented also in a spreadsheet (LibreOffice Calc 7.1.8.1) to demonstrate the model's accessibility. The spreadsheet is provided in xlsx-format as Supporting information.

3 Results

The case example based on a fed-batch process reported earlier⁸ is initialized first (Section 3.1). Determination of mixing time and substrate feed rate using a threshold substrate concentration at the feed point is demonstrated in Section 3.2. The minimum required oxygen transfer rates or oxygen gas partial pressures that avoid dissolved oxygen limitation are then evaluated (Section 3.3). Analysis of substrate or oxygen concentrations given a mixing time (or dispersion coefficient and geometry), substrate feed rate, oxygen transfer rate coefficient, and yield coefficients has been demonstrated earlier²⁵, and step-by-step analysis instructions have also been provided earlier³⁵.

3.1 Initializing the case example

One of the most cited bioprocess scale-up issues is the acetate overflow metabolism exhibited by *E. coli*. The production and consumption of acetate are eventually balanced by *E. coli*, and high glucose concentrations equilibrate these rates at high acetate concentrations²⁸. Thus, acetate accumulation is observed with high glucose concentrations, as the acetate concentration is rising towards its equilibrium concentration. For example, the 22 m³ *E. coli* fed-batch⁸ was reported to have a volumetric mean acetate concentration of 37 mg L⁻¹ with 20 g L⁻¹ biomass concentration at 20 h since the start of the process. An acetate concentration of 124 mg L⁻¹, a tenth of the acetate inhibition constant in the used kinetic model, was used here. Based on the *E. coli* W3110M model²⁸ used here, the 124 mg L⁻¹ acetate concentration corresponds to a 68.9 mg L⁻¹ glucose concentration with non-limiting oxygen. With 124 mg L⁻¹ acetate the maximal specific substrate uptake rate was $q_{S_{\max}} = 0.578 \text{ g g}^{-1}\text{h}$.

The gas-phase concentration of oxygen at the top of the reactor, O_G , was calculated with ideal gas equation assuming 21 mol-% oxygen content in the air. The resulting concentration $O_G \approx 656 \text{ mg L}^{-1}$ in the gas phase corresponded to a dissolved oxygen concentration of $O_L \approx 18.0 \text{ mg L}^{-1}$ at equilibrium. Hydrostatic pressure increased the equilibrium dissolved oxygen concentration to $O_L \approx 23.0 \text{ mg L}^{-1}$ at the bottom of the reactor (7 m depth). Oxygen limitation can be considered to occur when the dissolved oxygen concentration O_L equals the affinity constant (0.1 mg L⁻¹ here²⁸).

3.2 Maintaining substrate concentration below a limit

In an *E. coli* fed-batch process design context, one might ask what are the conditions for mixing time or glucose feed rate for preventing acetate accumulation or local oxygen depletion beyond a predetermined limit. Using the diffusion equation based model, the procedure for finding such a mixing time or feed rate is:

1. Decide on the upper limit for substrate.
 - The kinetic model can be used to relate the substrate value to the concentration of an unwanted side-product, such as acetate in the case example.
2. As a worst case scenario, assume a top feed ($x_0 = 1$)
 - The best-mixing feed at the middle follows this same procedure but with the mixing time reduced to a quarter³⁶⁻³⁸ of the mixing time corresponding to the top feed.
3. Calculate mean concentration of substrate and the substrate modulus using Eqns 6 and 5.
 - If the mixing time is being calculated:
 - (1) Calculate the mean concentration $\langle S \rangle$.
 - (2) Iterate the modulus M until the calculated substrate concentration at the feed point (Eqn 10) matches the maximum allowed concentration, S_{\max} .

- If the feed rate is being calculated:
 - (1) Make an initial guess for the feed rate Q_S first.
 - (2) Calculate the mean concentration $\langle S \rangle$ and modulus M .
- 4. Either:
 - (a) Calculate 95 % mixing time t_{95} using Eqn 11.
 - (b) Iterate feed rate Q_S until the substrate concentration S calculated with Eqn 10 matches the maximum allowed concentration.

The procedure is exemplified next with the case example, where the $S_{\max} = 68.9 \text{ mg L}^{-1}$ maximum substrate concentration defined in Section 3.1 is related to the highest allowed mixing time t_{95} or feed rate Q_S . An *xlsx* spreadsheet example of the procedure is also provided as Supporting information. Using a top feed ($x_0 = 1$), a worst-case scenario in terms of mixing, in Eqn 3 results in

$$S_{\max} = \langle S \rangle \frac{M}{\tanh M}. \quad (10)$$

(If $M \geq 1.86$, then $S_{\max} \approx \langle S \rangle M$ with less than 5 % error.)

With the considered exponential feed (Eqn 9), the mean substrate concentration (Eqn 6) was $\langle S \rangle = 27.2 \text{ mg}$, or 86.2 % of the allowed maximum concentration, leaving only a small margin for heterogeneity. The corresponding substrate modulus was $M = 2.49$ with the exponential feed regardless of considered biomass concentration. With the constant $Q_S = 4 \text{ g L}^{-1} \text{ h}^{-1}$ feed the mean substrate concentration ranged from the values exceeding the allowed 68.9 mg L^{-1} maximum with low biomass concentrations down to $\langle S \rangle = 7.7 \text{ mg L}^{-1}$ at $X = 40 \text{ g L}^{-1}$. The corresponding substrate moduli ranged from 0 to 8.89 with the constant feed depending on the biomass concentrations.

The mixing times were then calculated to range from 233 s to 23.3 s with the exponential feed and from 0 s to 206 s with the constant feed (Figure 1):

$$t_{95} = \frac{\pi}{\ln 40} \sqrt{t_{95} \frac{Q_S}{\langle S \rangle}}. \quad (11)$$

With the constant feed, the allowed mixing time was initially zero (infinite rate of mixing) or very low, as the feed rate Q_S was high with respect to the considered biomass concentration X , leading to high mean concentrations $\langle S \rangle$ as well with little to no margin for heterogeneity. At $X \approx 34 \text{ g L}^{-1}$ the constant $Q_S = 4 \text{ g L}^{-1}$ feed rate demanded the 165 s mixing time reported¹⁷ for the referenced large-scale experiment⁸. With the exponential feed, which is proportional to the biomass concentration, higher feed rates demanded lower mixing times to avoid acetate accumulating beyond the chosen 124 mg L^{-1} limit. Even though the mean concentration remained the same, the overall reaction rate increased for the higher biomasses. This led to stronger competition between reaction and mixing, demanding lower mixing times for the substrate to stay within the limit. The reported¹⁷ 165 s mixing time could support only an approximately $1.4 \text{ g L}^{-1} \text{ h}^{-1}$ feed rate or 6 g L^{-1} biomass concentration under the exponential scheme (Eqn 9). For most of the time, the referenced large-scale culture⁸ exceeded the limits calculated here.

Similarly, fixing the 95 % mixing time to a specified value, $t_{95} = 165 \text{ s}$ here¹⁷, allowed determining the highest substrate feed rates allowed by the 68.9 mg L^{-1} limit at the feedpoint. The mean concentration influences the modulus, but the modulus dictates which mean concentration is allowed by the substrate concentration limit. Direct computation of substrate's mean concentration and substrate modulus was thus not possible, but they

had to be calculated iteratively instead. The substrate feed rate was iterated to satisfy

$$S_{\max} - \langle S \rangle \frac{M}{\tanh M} = 0, \quad (12)$$

where both the mean $\langle S \rangle$ (Eqn 6) and modulus M (Eqn 5) depended on the feed rate Q_S . The mean concentration depended also on the biomass concentration X . The calculated substrate feed rates were between $1.59 \text{ g L}^{-1} \text{ h}^{-1}$ and $4.42 \text{ g L}^{-1} \text{ h}^{-1}$ with the 4 g L^{-1} to 40 g L^{-1} biomass (Figure 2A), and corresponding exponential growth rates (h^{-1}) are shown in Figure 2B. The corresponding allowed specific growth rates in an exponential feed (Eqn 9) would have been 0.10 h^{-1} at 7 g L^{-1} biomass concentration and down to 0.04 h^{-1} at 40 g L^{-1} biomass concentration. The obtained mean concentrations ranged from 24.0 mg L^{-1} at low biomass concentrations down to 8.8 mg L^{-1} at 40 g L^{-1} biomass concentration, and the corresponding extremes of modulus were 2.85 and 7.87.

Figure 3 demonstrates the axial substrate profiles (Eqn 3) obtained at $X = 20 \text{ g L}^{-1}$ with an optimized $t_{95} = 81 \text{ s}$ mixing time and an optimized $Q_S = 3.0 \text{ g L}^{-1}$ feed rate that satisfy the 68.9 mg L^{-1} substrate limit at the feed point. A reference profile is also shown with $t_{95} = 165 \text{ s}$, $Q_S = 4 \text{ g L}^{-1} \text{ h}^{-1}$, and $X = 20 \text{ g L}^{-1}$. The reference profile exceeded the considered substrate limit.

3.3 Maintaining dissolved oxygen concentration above limitation

Similarly to the previous Section 3.2, one could ask in a fed-batch process design context, what is the minimum required oxygen transfer rate coefficient $k_L a$ or oxygen gas partial pressure p_{O_G} for preventing oxygen limitation at the feed point's vicinity. The procedure for finding such oxygen transfer rate coefficients or oxygen gas partial pressures is:

1. Define the minimum limit for dissolved oxygen concentration.
2. Calculate the substrate's mean concentration $\langle S \rangle$ (Eqn 6), substrate modulus M (Eqn 5), and maximum concentration at feed point S_{\max} (Eqn 10).
3. Calculate oxygen consumption rate by using a kinetic model.
 - If no kinetic model is available, use a zeroth-order approximation²⁵, where the substrate feed rate Q_S is directly converted to a reactor-level volumetric oxygen consumption rate ($\text{g L}^{-1} \text{ h}^{-1}$) and weighted spatially by the substrate's axial profile $S/\langle S \rangle$ for local estimation.
4. Either:
 - (a) Calculate the oxygen transfer rate coefficient $k_L a$ using Eqn 13.
 - (b) Calculate the oxygen gas partial pressure p_{O_G} using Eqns 14 and 15.

This procedure is demonstrated with the case example using both a constant $Q_S = 4 \text{ g L}^{-1}$ and an exponential feed rate (Eqn 9). Both feed scenarios were considered with $t_{95} = 165 \text{ s}$ mixing time. A dissolved oxygen limit of 0.1 mg L^{-1} at the feed point ($x_0 = 1$) was chosen, which equaled the kinetic model's²⁸ affinity constant for oxygen.

With the exponential feed the substrate's mean concentration was $\langle S \rangle = 24.0 \text{ mg L}^{-1}$, but the substrate modulus M ranged from 2.24 at 4 g L^{-1} biomass to 7.08 at 40 g L^{-1} . Correspondingly the substrate's maximum concentration S_{\max} ranged from 54.9 mg L^{-1} to 170 mg L^{-1} , resulting in specific oxygen consumption rates q_O of $0.230 \text{ g g}^{-1} \text{ h}^{-1}$ to $0.323 \text{ g g}^{-1} \text{ h}^{-1}$ at the feed point. With the constant $Q_S = 4 \text{ g L}^{-1} \text{ h}^{-1}$ feed the substrate's mean concentration was between 6.9 mg L^{-1} and 107 mg L^{-1} , the substrate modulus between 2.13 and 8.40, and the substrate's maximum concentration between 58.4 mg L^{-1} and 236 mg L^{-1} . The specific oxygen consumption rate was between $0.222 \text{ g g}^{-1} \text{ h}^{-1}$ and 0.306 mg L^{-1} . With exponential feed the highest

specific oxygen consumption occurred at 40 g L^{-1} , where the substrate feed rate and maximum substrate concentration were also highest ($9.8 \text{ g L}^{-1} \text{ h}^{-1}$). In contrast, with constant $4 \text{ g L}^{-1} \text{ h}^{-1}$ feed the 40 g L^{-1} biomass had the lowest q_O .

Using these values, the required oxygen transfer rate coefficients shown in Figure 4 were calculated with

$$k_{La} = \frac{q_O X}{h_O O_G - O_L}, \quad (13)$$

which was derived from the oxygen's local steady-state balance Eqn 7. With the constant $4 \text{ g L}^{-1} \text{ h}^{-1}$ feed the oxygen transfer rate coefficient k_{La} required to avoid limitations was between 170 h^{-1} and 495 h^{-1} . With the exponential feed 51.3 h^{-1} to 721 h^{-1} transfer rate coefficients were required. The reference cultivation's $k_{La} = 180 \text{ h}^{-1}$ was sufficient with 10 g L^{-1} biomass with constant feed or approximately 12 g L^{-1} biomass with exponential feed. As an alternative, the required oxygen gas concentrations to avoid limitation with $k_{La} = 180 \text{ h}^{-1}$ were calculated with

$$O_G = \frac{1}{h_O} \left(O_L + \frac{q_O X}{k_{La}} \right), \quad (14)$$

which also resulted directly from the dissolved oxygen's balance Eqn 7. The gas concentrations were transformed to corresponding partial pressures (Figure 5) with the ideal gas equation:

$$p_{O_G} = \frac{O_G}{RT}. \quad (15)$$

With the constant feed, oxygen gas partial pressures of 499 mbar to 1440 mbar were required, which was mostly above the 525 mbar level in the reference cultivation⁸. With the exponential feed, 152 mbar to 2090 mbar partial pressures were required. Similarly to Section 3.2, one could also define the highest allowed mixing time or feed rate given an oxygen transfer rate coefficient and oxygen gas partial pressure.

Figure 6 shows axial profiles of dissolved oxygen with the optimized oxygen transfer rate coefficients and oxygen gas partial pressures that satisfy the 0.1 mg L^{-1} dissolved oxygen concentration limit at the feed point. A profile matching the reference cultivation⁸ with $k_{La} = 180 \text{ h}^{-1}$ and $p_{O_G} = 525 \text{ mbar}$ is also shown. Approximately 20 % of the reference profile was below the 0.1 mg L^{-1} limit.

4 Discussion

Section 4.1 discusses the effect of the assumptions and simplifications on the results. Practical consequences of the modeling results are treated in Section 4.2. Section 4.3 concludes by reflecting the results with the study's goals.

4.1 Effect of assumptions

All the above analyses assumed that the substrate's mean concentration $\langle S \rangle$ can be determined accurately by applying a steady-state assumption directly to the kinetic model where the substrate consumption rate was of the Monod-form²⁹. The simple and straightforward approach has two concerns:

(1) Assumption of homogeneous substrate concentration in the kinetic equations. For consistency, the substrate feed rate should match a spatially averaged substrate consumption rate

$$Q_S = X \int_0^1 q_S(S(x)) dx, \quad (16)$$

where the axially variable substrate concentration obeys Eqn 3. However, the local substrate concentration S depends on the mean concentration $\langle S \rangle$ in Eqn 3. The substrate's axial profile, the mean, and thus the modulus are interdependent. The coupled quantities can be resolved by iterating *e.g.* the mean concentration until Eqn 16 holds (Supporting information). This is a source for potential error in the shown calculations: in the reference state $X = 20 \text{ g L}^{-1}$, $Q_S = 4 \text{ g L}^{-1} \text{ h}^{-1}$, and $t_{95} = 165 \text{ s}$, the mean $\langle S \rangle$ was 19.6 mg L^{-1} with homogeneity assumption but 28.9 mg L^{-1} (48 % higher) with the heterogeneity correction (Eqn 16). Similarly, the highest allowed acetate and substrate concentrations were connected with the kinetic model using homogeneous concentration profiles for the sake of demonstration, and accounting for heterogeneity at the level of the kinetic model requires iteration of integral equations similar to Eqn 16.

(2) Steady-state violation. Especially with relatively low biomass concentrations, the time derivative of the mean concentration is not necessarily zero. Here, the steady-state assumption led to negative substrate mean concentrations $\langle S \rangle$ with the constant $4 \text{ g L}^{-1} \text{ h}^{-1}$ feed at biomass concentrations of 6 g L^{-1} and below, which implies that accumulation of substrate should have occurred and that the overall volumetric reaction rate in the modulus should have been lower than the substrate feed rate. Also, with high feed rates the dilution term might reduce the mean concentration's value. If required, it is relatively straightforward to apply a transient balance equation with or without dilution to substrate:

$$\frac{d\langle S \rangle}{dt} = -\langle q_S \rangle X - D \langle S \rangle + Q_S. \quad (17)$$

The transient balance can be used with either a homogeneous or heterogeneous substrate concentration such that either $\langle q_S \rangle = q_S(\langle S \rangle)$ or $\langle q_S \rangle = \int_0^1 q_S(x) dx$: the specific substrate uptake rate q_S depends on the local substrate concentration S , which can be calculated directly from the prevailing mean concentration $\langle S \rangle$ (Eqn 3). The direct $q_S = q_S(S(x))$ calculation does assume a local steady-state, though.

4.2 Practical consequences

With the exponential feed only a $t_{95} = 23.3 \text{ s}$ (14.1 % mixing time of the original 165 s) would have been allowed at $X = 40 \text{ g L}^{-1}$ biomass concentration. The well-established connection between mixing times and specific stirrer power input,^{27,39,40} $t_{95} \sim \epsilon^{-1/3}$, implies that this would require a 357-fold stirrer power input (463 W kg^{-1}), which is entirely unrealistic. With a constant feed the maximum allowed mixing time was 206 s with 40 g L^{-1} , which would have allowed a 20 % reduction in the mixing time, corresponding to using half of the original 1.3 W kg^{-1} stirrer power input. Most of the process time is usually not spent on maximal biomass concentration, though, but the mixing times required for staying within the substrate concentration limit were not feasible for most of the considered biomass concentration interval. This implies that either the acetate and thus substrate concentration limits should be relaxed in the example case or another approach be implemented that is not based on increasing stirrer power. According to previous simulations, such mixing time improvements could be feasible with multi-point feeds³⁶, also enabling higher productivities through the use of higher feed rates. Using a middle feed $x_0 = 0.5$ instead of a top feed would also divide the mixing time by four^{24,37} and the substrate modulus by two (Eqn 5), relaxing the requirements.

Similarly to the mixing times necessary to avoid excessive substrate concentrations at the feed point, $k_L a$ values of up to 720 h^{-1} —untypical under the studied large-scale conditions—would have been required to avoid oxygen limitations. According to a previous review⁴¹ covering reactor sizes up to 2.6 m^3 , the oxygen transfer rate coefficient scales with specific power input by $k_L a \sim \epsilon^{0.4}$ to $k_L a \sim \epsilon^{1.1}$. A more recent mechanistic scale-up correlation⁴² suggests an approximately $k_L a \sim \epsilon^{0.5}$ scaling. These suggest, that avoiding oxygen limitation by increasing the transfer rate coefficient from the reported⁸ 180 h^{-1} up to 721 h^{-1}

calculated here would require an up to 32-fold power input, which is not feasible at an industrial scale. As with the mixing time, either the chosen dissolved oxygen limits need to be relaxed or another approach be chosen. Alternatively, increasing the pressure scales linearly with the required compressor power. Therefore, increasing the oxygen gas partial pressure from the reference 525 mbar up to the 2090 mbar calculated here would require a $2090/525 \approx 4$ -fold compressor power input. In the context of the reference cultivation, this would correspond to increasing the head-space pressure to approximately 5 bar. In terms of operating expenses, increasing the oxygen partial pressure scales thus more favourably than increasing the stirrer power input for a higher transfer rate coefficient. Their differing effects on capital expenses need to be remembered, of course, but accounting for them is not attempted here.

4.3 Conclusion and future outlook

Earlier studies have demonstrated how the presented diffusion equation modeling can be applied to analyze profiles of substrate, oxygen, carbon dioxide, temperature, and pH in large-scale fed-batch bioprocesses^{24,25,35}. Numerical simulations with computational fluid dynamics or compartment modeling approaches require initialization of the values to be calculated, and typically a homogeneous initial distribution is chosen^{18,19} for simplicity. The simple diffusion equation based analyses demonstrated earlier and also partly here (Figures 3 and 6) could be used to improve the convergence of simulations by providing a heterogeneous initial estimate. Likewise, directly computed operating conditions satisfying a predefined constraint, *e.g.* the avoidance of acetate accumulation as demonstrated here (Section 3.2), could be used as the operating parameters for numerical simulations. In the context of scale-down reactor design, the simple diffusion equation based modeling could provide a quick and computationally low-cost estimate of the conditions that the microorganisms are expected to face in large-scale reactors.

The current work focused on expanding the model's use to answering practical design questions related to bioprocess scale-up, optimization, and intensification. Determination of highest mixing times, substrate feed rates, and exponential feed rates that avoid acetate accumulation beyond a limit according to a kinetic model was illustrated. Likewise, the model was applied here to define oxygen transfer rate coefficients and oxygen gas partial pressures required to avoid oxygen limitation at the feed point's vicinity. The model and the applied design perspective identified that unrealistically low mixing times and high oxygen transfer rates would be required to avoid acetate accumulation and oxygen limitation in the referenced⁸ large-scale fed-batch. Relocating the feed point or using multiple feed points and increasing the overall pressure seemed more favourable approaches. In conclusion, it is possible to use the model to directly deduce operating conditions using the desired end result as the starting point as suggested previously²². Operating procedures for the shown analyses were provided to facilitate model application.

Unlike compartment models, the diffusion equation based model is simple enough to be implemented in a spreadsheet (Supporting information). On the downside, many simplifications are required, but this is usually acceptable when the purpose of the modeling is to aid preliminary design. Potential future improvements for the diffusion equation based model include (1) using it also to answer design questions related to CO₂, temperature, and pH levels, (2) studying its application for assessing the cellular lifelines, which has proved essential for scaling down a large-scale bioprocess^{18,19,22}, (3) studying the coupling between cellular maintenance rate and substrate heterogeneity⁴³, and (4) the refinement of the dispersion coefficient or mixing time prediction methodology to enhance the model's applicability in scenarios lacking experimental mixing data, (5) studying the model's applicability in describing pneumatically agitated large-scale bioreactors.

Supporting information

Supplementary file: An xlsx-example for Sections 3.2 and 4.1.

References

1. Nadal-Rey G, McClure DD, Kavanagh JM, Cornelissen S, Fletcher DF and Germaey KV. Understanding gradients in industrial bioreactors. *Biotechnol Adv* **46**: 107660 (2021). doi:10.1016/j.biotechadv.2020.107660.
2. Caspeta L, Flores N, Pérez NO, Bolívar F and Ramírez OT. The effect of heating rate on *Escherichia coli* metabolism, physiological stress, transcriptional response, and production of temperature-induced recombinant protein: A scale-down study. *Biotechnol Bioeng* **102**: 468–482 (2009). doi:10.1002/bit.22084.
3. Cortés JT, Flores N, Bolívar F, Lara AR and Ramírez OT. Physiological effects of pH gradients on *Escherichia coli* during plasmid DNA production. *Biotechnol Bioeng* **113**: 598–611 (2016). doi:10.1002/bit.25817.
4. Schweder T, Krüger E, Xu B, Jörgen B, Blomsten G, Enfors S-O and Hecker M. Monitoring of genes that respond to process-related stress in large-scale bioprocesses. *Biotechnol Bioeng* **65**: 151–159 (1999). doi:10.1002/(SICI)1097-0290(19991020)65:2<151::AID-BIT4>3.0.CO;2-V.
5. Lara AR, Leal L, Flores N, Gosset G, Bolívar F and Ramírez OT. Transcriptional and metabolic response of recombinant *Escherichia coli* to spatial dissolved oxygen tension gradients simulated in a scale-down system. *Biotechnol Bioeng* **93**: 372–385 (2006). doi:10.1002/bit.20704.
6. Gecse G, Vente A, Kilstrup M, Becker P and Johanson T. Impact of Elevated Levels of Dissolved CO₂ on Performance and Proteome Response of an Industrial 2'-Fucosyllactose Producing *Escherichia coli* Strain. *Microorganisms* **10**: 1145 (2022). doi:10.3390/microorganisms10061145.
7. Enfors S-O, Jahic M, Rozkov A, Xu B, Hecker M, Jürgen B, Krüger E, Schweder T, Hamer G, O'Beirne D, Noisommit-Rizzi N, Reuss M, Boone L, Hewitt C, McFarlane C, Nienow A, Kovacs T, Trägårdh C, Fuchs L, Revstedt J, Friberg PC, Hjertager B, Blomsten G, Skogman H, Hjort S, Hoeks F, Lin H-Y, Neubauer P, Van Der Lans R, Luyben K, Vrabel P and Manelius Å. Physiological responses to mixing in large scale bioreactors. *J Biotechnol* **85**: 175–185 (2001). doi:10.1016/S0168-1656(00)00365-5.
8. Xu B, Jahic M, Blomsten G and Enfors S-O. Glucose overflow metabolism and mixed-acid fermentation in aerobic large-scale fed-batch processes with *Escherichia coli*. *Appl Microbiol Biotechnol* **51**: 564–571 (1999). doi:10.1007/s002530051433.
9. George S, Larsson G, Olsson K and Enfors S-O. Comparison of the Baker's yeast process performance in laboratory and production scale. *Bioprocess Eng* **18**: 135–142 (1998). doi:10.1007/PL00008979.
10. Bylund F, Castan A, Mikkola R, Veide A and Larsson G. Influence of scale-up on the quality of recombinant human growth hormone. *Biotechnol Bioeng* **69**: 119–128 (2000). doi:10.1002/(SICI)1097-0290(20000720)69:2<119::AID-BIT1>3.0.CO;2-9.
11. Puiman L, Almeida Benalcázar E, Picioreanu C, Noorman HJ and Haringa C. High-resolution computation

predicts that low dissolved CO concentrations and CO gradients promote ethanol production at industrial-scale gas fermentation. *Biochem Eng J* **207**: 109330 (2024). doi:10.1016/j.bej.2024.109330.

12. Velastegui E, Quezada J, Guerrero K, Altamirano C, Martinez JA, Berrios J and Fickers P. Is heterogeneity in large-scale bioreactors a real problem in recombinant protein synthesis by *Pichia pastoris*? *Appl Microbiol Biotechnol* **107**: 2223–2233 (2023). doi:10.1007/s00253-023-12434-2.

13. Bisgaard J, Zahn JA, Tajssoleiman T, Rasmussen T, Huusom JK and Gernaey KV. Data-based dynamic compartment model: Modeling of *E. coli* fed-batch fermentation in a 600 m³ bubble column. *J Ind Microbiol Biotechnol* **49**: kuac021 (2022). doi:10.1093/jimb/kuac021.

14. Ngu V, Fletcher DF, Kavanagh JM, Rafrafi Y, Dumas C, Morchain J and Cockx A. H₂ mass transfer – A key factor for efficient biological methanation: Comparison between pilot-scale experimental data, 1D and CFD models. *Chem Eng Sci* **268**: 118382 (2023). doi:10.1016/j.ces.2022.118382.

15. Ngu V, Morchain J and Cockx A. Spatio-temporal 1D gas–liquid model for biological methanation in lab scale and industrial bubble column. *Chem Eng Sci* **251**: 117478 (2022). doi:10.1016/j.ces.2022.117478.

16. Pigou M and Morchain J. Investigating the interactions between physical and biological heterogeneities in bioreactors using compartment, population balance and metabolic models. *Chem Eng Sci* **126**: 267–282 (2015). doi:10.1016/j.ces.2014.11.035.

17. Vrabel P, Van Der Lans RGJM, Van Der Schot FN, Luyben KChAM, Xu B and Enfors S-O. CMA: Integration of fluid dynamics and microbial kinetics in modelling of large-scale fermentations. *Chem Eng J* **84**: 463–474 (2001). doi:10.1016/S1385-8947(00)00271-0.

18. Haringa C. An analysis of organism lifelines in an industrial bioreactor using Lattice-Boltzmann CFD. *Eng Life Sci* **23**: e2100159 (2023). doi:10.1002/elsc.202100159.

19. Haringa C, Tang W, Wang G, Deshmukh AT, Van Winden WA, Chu J, Van Gulik WM, Heijnen JJ, Mudde RF and Noorman HJ. Computational fluid dynamics simulation of an industrial *P. chrysogenum* fermentation with a coupled 9-pool metabolic model: Towards rational scale-down and design optimization. *Chem Eng Sci* **175**: 12–24 (2018). doi:10.1016/j.ces.2017.09.020.

20. Nauha EK, Kalal Z, Ali JM and Alopaeus V. Compartmental modeling of large stirred tank bioreactors with high gas volume fractions. *Chem Eng J* **334**: 2319–2334 (2018). doi:10.1016/j.cej.2017.11.182.

21. Morchain J, Gabelle J and Cockx A. A coupled population balance model and CFD approach for the simulation of mixing issues in lab-scale and industrial bioreactors. *AIChE J* **60**: 27–40 (2014). doi:10.1002/aic.14238.

22. Noorman HJ and Heijnen JJ. Biochemical engineering’s grand adventure. *Chem Eng Sci* **170**: 677–693 (2017). doi:10.1016/j.ces.2016.12.065.

23. Szenk M, Dill KA and De Graff AMR. Why do fast-growing bacteria enter overflow metabolism? Testing the membrane real estate hypothesis. *Cell Syst* **5**: 95–104 (2017). doi:10.1016/j.cels.2017.06.005.

24. Losoi P, Konttinen J and Santala V. Modeling large-scale bioreactors with diffusion equations. Part I: Predicting axial dispersion coefficient and mixing times. *Biotechnol Bioeng* **121**: 1060–1075 (2024). doi:10.1002/bit.28632.
25. Losoi P, Konttinen J and Santala V. Modeling large-scale bioreactors with diffusion equations. Part II: Characterizing substrate, oxygen, temperature, carbon dioxide, and pH profiles. *Biotechnol Bioeng* **121**: 1102–1117 (2024). doi:10.1002/bit.28635.
26. Vasconcelos JMT, Alves SS, Nienow AW and Bujalski W. Scale-up of mixing in gassed multi-turbine agitated vessels. *Can J Chem Eng* **76**: 398–404 (1998). doi:10.1002/cjce.5450760308.
27. Vrabel P, Van Der Lans RGJM, Luyben KChAM, Boon L and Nienow AW. Mixing in large-scale vessels stirred with multiple radial or radial and axial up-pumping impellers: Modelling and measurements. *Chem Eng Sci* **55**: 5881–5896 (2000). doi:10.1016/S0009-2509(00)00175-5.
28. Anane E, Lopez C DC, Neubauer P and Cruz Bournazou MN. Modelling overflow metabolism in *Escherichia coli* by acetate cycling. *Biochem Eng J* **125**: 23–30 (2017). doi:10.1016/j.bej.2017.05.013.
29. Monod J. The growth of bacterial cultures. *Annu Rev Microbiol* **3**: 371–394 (1949). doi:10.1146/annurev.mi.03.100149.002103.
30. Sander R. Compilation of Henry’s law constants (version 5.0.0) for water as solvent. *Atmos Chem Phys* **23**: 10901–12440 (2023). doi:10.5194/acp-23-10901-2023.
31. Korz DJ, Rinas U, Hellmuth K, Sanders EA and Deckwer W-D. Simple fed-batch technique for high cell density cultivation of *Escherichia coli*. *J Biotechnol* **39**: 59–65 (1995). doi:10.1016/0168-1656(94)00143-Z.
32. Harris CR, Millman KJ, Van Der Walt SJ, Gommers R, Virtanen P, Cournapeau D, Wieser E, Taylor J, Berg S, Smith NJ, Kern R, Picus M, Hoyer S, Van Kerkwijk MH, Brett M, Haldane A, Del Rıo JF, Wiebe M, Peterson P, Gerard-Marchant P, Sheppard K, Reddy T, Weckesser W, Abbasi H, Gohlke C and Oliphant TE. Array programming with NumPy. *Nature* **585**: 357–362 (2020). doi:10.1038/s41586-020-2649-2.
33. The pandas development team. Pandas-dev/pandas: Pandas. (2020). doi:10.5281/ZENODO.3509134.
34. McKinney W. Data Structures for Statistical Computing in Python. Austin, Texas, 2010., pp 56–61 doi:10.25080/Majora-92bf1922-00a.
35. Losoi P. *Characterization of large-scale bioreactors: Modeling biological and multi-point feed approaches to reactor homogenization*. Tampere University, 2024. <https://urn.fi/URN:ISBN:978-952-03-3226-6>.
36. Losoi P, Konttinen J and Santala V. Substantial gradient mitigation in simulated large-scale bioreactors by optimally placed multiple feed points. *Biotechnol Bioeng* **119**: 3549–3566 (2022). doi:10.1002/bit.28232.
37. Alves SS, Vasconcelos JMT and Barata J. Alternative compartment models of mixing in tall tanks agitated by multi-Rushton turbines. *Chem Eng Res Des* **75**: 334–338 (1997). doi:10.1205/026387697523642.

38. Vrabel P, Van Der Lans RGJM, Cui YQ and Luyben KChAM. Compartment model approach: Mixing in large scale aerated reactors with multiple impellers. *Chem Eng Res Des* **77**: 291–302 (1999). doi:10.1205/026387699526223.
39. Bernauer S, Eibl P, Witz C, Khinast J and Hardiman T. Analyzing the effect of using axial impellers in large-scale bioreactors. *Biotechnol Bioeng* **119**: 2494–2504 (2022). doi:10.1002/bit.28163.
40. Nienow AW. On impeller circulation and mixing effectiveness in the turbulent flow regime. *Chem Eng Sci* **52**: 2557–2565 (1997). doi:10.1016/S0009-2509(97)00072-9.
41. Garcia-Ochoa F and Gomez E. Bioreactor scale-up and oxygen transfer rate in microbial processes: An overview. *Biotechnol Adv* **27**: 153–176 (2009). doi:10.1016/j.biotechadv.2008.10.006.
42. Nauha EK, Visuri O, Vermasvuori R and Alopaeus V. A new simple approach for the scale-up of aerated stirred tanks. *Chem Eng Res Des* **95**: 150–161 (2015). doi:10.1016/j.cherd.2014.10.015.
43. Maluta F, Pigou M, Montante G and Morchain J. Modeling the effects of substrate fluctuations on the maintenance rate in bioreactors with a probabilistic approach. *Biochem Eng J* **157**: 107536 (2020). doi:10.1016/j.bej.2020.107536.

Figures

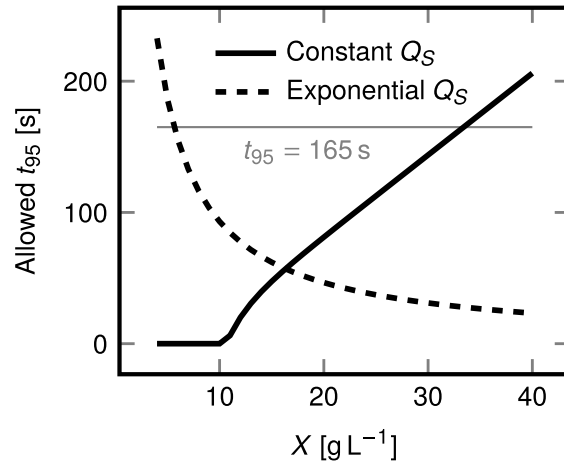


Figure 1: Figure 1: Highest allowed 95 % mixing times that maintain glucose concentration below the 68.9 mg L^{-1} limit in the reactor. A 165 s mixing time was reported¹⁷ for the reference cultivation⁸. Constant $Q_S = 4 \text{ g L}^{-1} \text{ h}^{-1}$, exponential $Q_S = (0.245 \text{ g g}^{-1} \text{ h}^{-1}) X$.

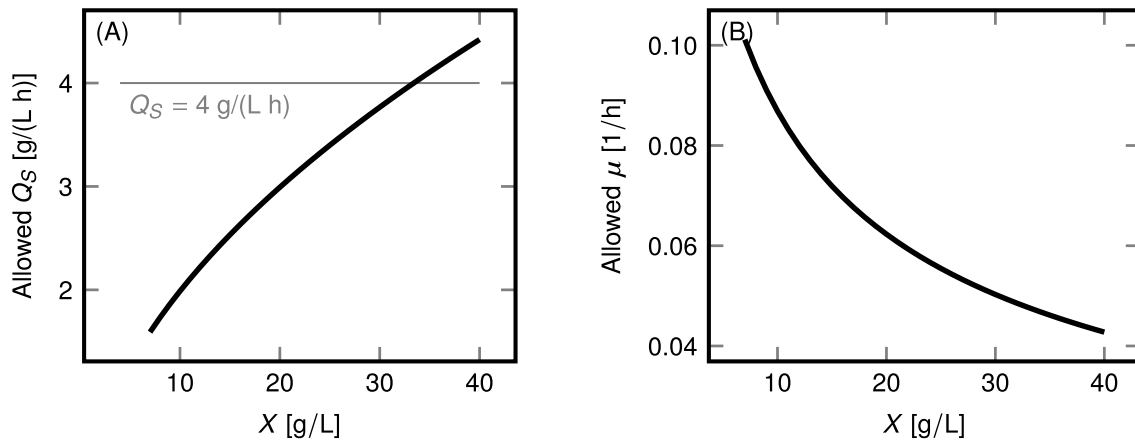


Figure 2: Figure 2: Highest allowed (A) constant glucose feed rates (B) and exponential feed rates that maintain glucose concentration below 68.9 mg L^{-1} in the reactor with $t_{95} = 165 \text{ s}$. An approximately $4 \text{ g L}^{-1} \text{ h}^{-1}$ substrate feed rate was used in the reference cultivation⁸.

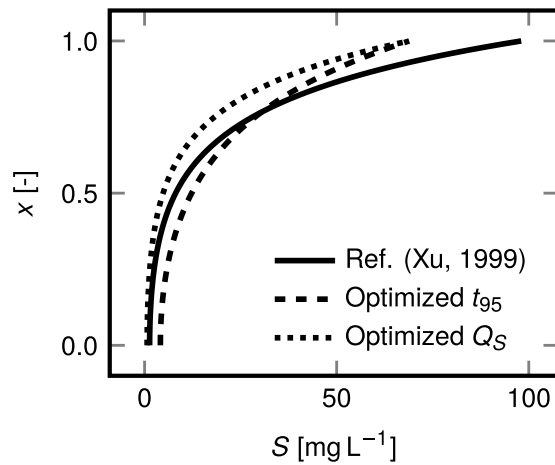


Figure 3: Figure 3: Substrate profiles with optimized mixing time and feed rate. The estimate for the reference cultivation⁸ has $t_{95} = 165 \text{ s}$ and $Q_S = 4 \text{ g L}^{-1} \text{ h}^{-1}$. Each profile has $X = 20 \text{ g L}^{-1}$.

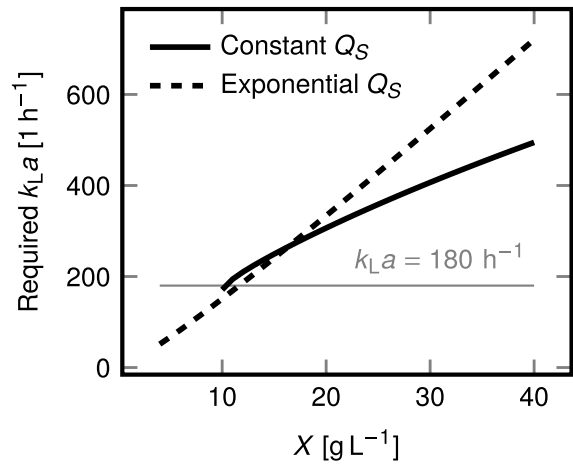


Figure 4: Figure 4: Required oxygen transfer rate coefficients that avoid oxygen limitation at the feed point with a 165 s mixing time and a 525 mbar oxygen gas partial pressure. The reference cultivation⁸ had $k_{La} = 180 \text{ h}^{-1}$. Constant $Q_S = 4 \text{ g L}^{-1} \text{ h}^{-1}$, exponential $Q_S = (0.245 \text{ g g}^{-1} \text{ h}^{-1}) X$.

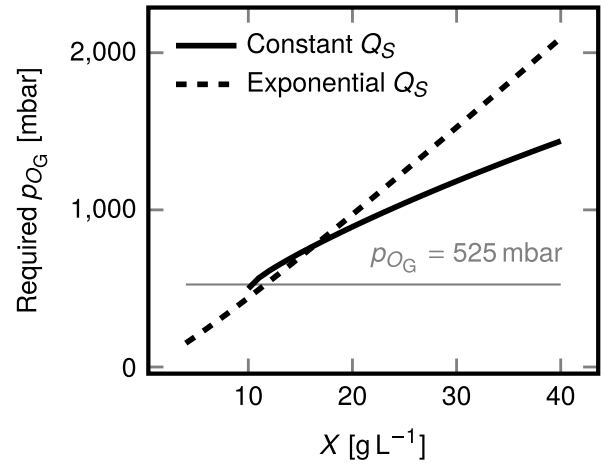


Figure 5: Figure 5: Required oxygen gas partial pressures that avoid oxygen limitation at the feed point with a 165 s mixing time and 180 h^{-1} oxygen transfer rate coefficient. The reference cultivation was estimated to have $p_{O_G} = 525 \text{ mbar}$. Constant $Q_S = 4 \text{ g L}^{-1} \text{ h}^{-1}$, exponential $Q_S = (0.245 \text{ g g}^{-1} \text{ h}^{-1}) X$.

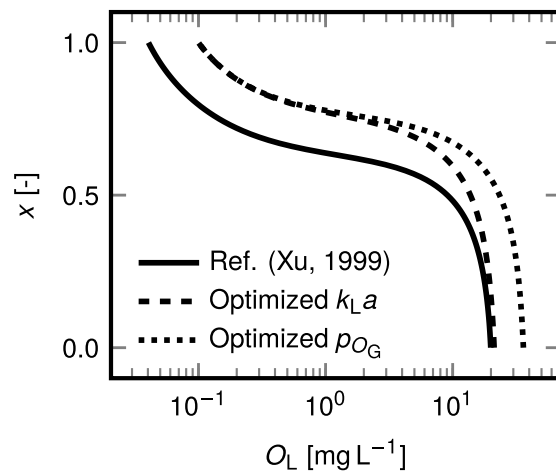


Figure 6: Figure 6: Dissolved oxygen profiles with optimized oxygen transfer rate coefficient and oxygen gas partial pressure. The estimate for the reference cultivation⁸ has $k_L a = 180 \text{ h}^{-1}$ and $p_{O_G} = 525 \text{ mbar}$. Each profile has $X = 20 \text{ g L}^{-1}$, $Q_S = 4 \text{ g L}^{-1} \text{ h}^{-1}$, and $t_{95} = 165 \text{ s}$.